AIAA JOURNAL
Vol. 32, No. 3, March 1994

Active Open-Loop Control of Particle Dispersion in Round Jets

Ellen K. Longmire*
University of Minnesota, Minneapolis, Minnesota 55455
and
John K. Eaton†
Stanford University, Stanford, California 94305

The objective of this study was to perturb vortex ring structures forming in the near field of a round air jet to modify the dispersion of solid particles in the flow. A jet with Reynolds number based on exit diameter of 1.9×10^4 was loaded with 55-μ diameter glass beads and forced axially with an acoustic speaker. Forcing waveforms were either single or double frequency. Results from flow visualization, laser Doppler anemometry, and quantitative mapping of particle number density show that significant modifications to local particle concentration and dispersion could be achieved.

Nomenclature

c = normalized particle number density
D = nozzle exit diameter
D_x = sum of cr over r beyond initial jet radius at a given x position
d_p = particle diameter
f = forcing frequency
Re_D = jet Reynolds number, $U_0 D/\nu$
Re_p = particle Reynolds number, $(U - V)d_p/\nu$
r = radial coordinate
St = Stokes number, τ_p/τ_f
St_D = Strouhal number, fD/U_0
U = local fluid velocity
U_0 = mean nozzle exit velocity
V, v' = mean and rms particle velocities, respectively
x = axial coordinate with origin at jet nozzle exit
Γ_x = sum of c over r at a given x position
Θ = relative phase between fundamental and subharmonic waves
Θ_m = shear layer momentum thickness
μ = dynamic viscosity
ν = kinematic viscosity
τ_f = eddy turnover time
τ_p = particle time constant

Introduction

PARTICLE-LADEN jet flows arise frequently in industrial applications where fine solids or liquid droplets must be injected into a combustion chamber, a process stream, or a reaction vessel. In many of these applications the system designer would like to modify or control the dispersion of particles. The present study is motivated by the desire to control combustion in coal-fired utility boilers where pulverized coal is conveyed by a portion of the combustion air entering the boiler as a jet. The dispersion rate of the coal particles directly affects the local environment surrounding each particle and therefore the combustion reaction kinetics. Although conventional boiler designs have been optimized empirically to maximize coal combustion efficiency, the fundamental fluid mechanics of the coal injection process and of particle-laden flow in general are as yet poorly understood. Current desires to minimize the levels of nitrogen oxides produced in coal combustors have led us to study the fundamental fluid mechanics and the possibility of controlling particle motions by controlling turbulence structure.

Over the last 20 years, studies on single-phase jets have provided a wealth of information about the temporal flow structure. Many experiments[1,2] have shown that coherent structures form in the near field of round jets. Axisymmetric structures (vortex rings) are usually dominant up to $x/D = 4$. Beyond the jet core, helical instabilities have a stronger growth rate so that organized helical structures may become important.[3] Coherent structures have been found in jets with very high Reynolds numbers[4] and in jet flames.[5]

A round jet is an example of a convectively unstable flow where the effects of instabilities occurring near the jet origin convect downstream and may become amplified. According to Koch et al.,[6] the appropriate means to control a convectively unstable flow is an open-loop system or a system where no feedback mechanism is involved. Remarkable degrees of control of a jet structure have been implemented by perturbing the structures that naturally occur in the jet near field. Examples of passive control of a jet structure (control where no energy is added to the flow) include the work of Ho and Gutmark[7] on elliptic jets and Wlezien and Kibens[8] on jets with indeterminate origin nozzles. Examples of active control (control where energy is added to the flow) include work in forced jets[9,10] and bifurcating and blooming jets.[11] In these experiments, acoustic speakers or mechanical manipulation were used to perturb the initial shear layer of the jet to generate repeatable vortex rings. Energy was added to the flow at frequencies other than the most unstable frequency to vary the length scale of the rings formed. Furthermore, Ho and Huang[12] showed in a two-dimensional mixing layer that forcing at frequencies much lower than the most unstable frequency predicted by linear stability analysis could be used to cause collective interactions. Then, several small vortices coalesce immediately after formation so that the vortex passage frequency is quickly reduced to the forcing frequency.

Arbey and Ffowcs Williams[13] forced a jet simultaneously with two frequencies, a fundamental plus the first subharmonic. This strategy yielded vortex formation at the forcing frequency and an eventual pairing of vortices. The authors demonstrated that, by varying the relative phase between the two forcing waves, the nature of vortex pairing could be controlled. In addition, a theoretical analysis by Mankbadi[14] and experiments by Husain et al.[15] showed that the relative phase between the waves affects the axial location of pairing.

Recent work in particle-laden flows has demonstrated that when particles have inertial time scales on the same order of magnitude as fluid eddy time scales, particle motions can be strongly affected by the eddies. A particle time scale based on Stokes flow is $\tau_p = \rho_p d_p^2/(18\mu)$, whereas an appropriate fluid time scale is an eddy turnover time based on eddy length divided by propagation vel-

Received Feb. 17, 1993; revision received Aug. 20, 1993; accepted for publication Aug. 23, 1993.

*Assistant Professor, Department of Aerospace Engineering and Mechanics. Member AIAA.
†Professor, Department of Mechanical Engineering. Member AIAA.

ocity. The ratio of these time scales is defined as the Stokes number St. Experiments by Lazaro and Lasheras[16] and Kamalu et al.[17] in particle-laden two-dimensional mixing layers showed that when $St \sim 1$ the concentration of particles was much higher in vortex braid regions than in vortex core regions. In a separate paper,[18] the present authors reported on the structure of a particle-laden jet flow where particles were found to concentrate in the regions of high strain downstream of vortex ring cores. The dominant mechanism for particle dispersion was shown to be the convection of particles by outwardly moving fluid downstream of vortex cores. This behavior persisted even when the particle-to-air mass loading ratio was increased up to 0.65.

Given the correlations between particle distribution and fluid structure observed in the previous studies, it seems likely that particle distributions can be modified by altering the otherwise typical coherent structures in a flow. In the present experiments, the particle-laden jet was forced axially with either a single frequency or a fundamental plus a subharmonic. The objectives were to generate vortices of varying length scale and to cause vortex pairing at specific axial locations in a particle-laden jet. Resulting distributions and velocities of particles were then examined.

Experimental Facility

Experiments were conducted in the facility shown in Fig. 1 with the flow directed vertically downward. (The facility and experimental methods are described in detail in Longmire and Eaton.[18,19]). Pressurized air passed through either a fluidized bed of particles or a bypass line. Particle and air streams were mixed and entered the 2- in. diam plenum through opposed outlets. In the plenum, the flow passed through a perforated plate and an axisymmetric contraction with an area ratio of 6.45:1 and an exit diameter of 2 cm. The perforated plate was removed for laser Doppler anemometry (LDA) measurements because particles tended to accumulate on the plate over longer periods of time. Also, a splitter plate was inserted between the two flow inlets for LDA measurements. The plate improved flow steadiness over long periods of time by preventing unstable interaction of the flow from the opposing jets entering the plenum. For the present experiments, the nozzle exit velocity was 14.4 m/s, yielding $Re_D = 1.9 \times 10^4$.

An audio speaker at the upstream end of the plenum induced velocity perturbations at the jet exit. Forcing waveforms were generated by an IBM XT computer containing a Data Translation 2801 acquisition and control card. Resulting analog signals were sent through a low-pass filter and an audio amplifier before reaching the speaker. In general, the flow was forced at large amplitudes to impose a strong oscillating component on the velocity at the jet exit. Large amplitudes were required to cause the collective interactions necessary to generate repeatable vortex rings at the forcing frequency. Spectra computed from hot-wire measurements in the jet core were dominated by sharp peaks at the forcing frequency.

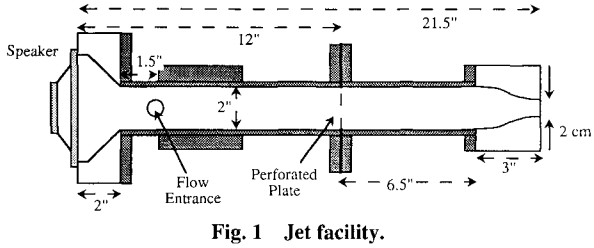

Fig. 1 Jet facility.

Spherical glass beads nominally sized between 50 and 60 μm by a centrifugal classifier constituted the particle phase of flow. Actual size distributions determined with a Coulter counter and a sonic sifter showed that 83% of the particle mass fell between 50 and 60 μm, and 95% of the mass fell between 45 and 65 μm. Average particle density was measured as 2.4 g/cm^3 yielding τ_p of 18–26 ms for particles between 50 and 60 μm. Particles were loaded into a fluidized bed, and air was injected into the bed through a porous sintered bronze plate below the freeboard. Particles that elutriated out the top of the bed were fed to the jet plenum. The mass loading ratio of particles to air in the flow was 5–11%.

Experimental Techniques

To mark the jet airflow, we introduced glycerine smoke into the air line through a venturi upstream of the jet plenum. A Plasma Kinetics 151 copper vapor laser was used to visualize either smoke or glass particles. The 1-in.-diam beam was formed into a thin (1 mm) sheet of light with a 400-mm cylindrical and a 1-m spherical lens and was aligned perpendicular to the nozzle exit. The laser emitted 30-ns light pulses of 3 mJ at a normal operating frequency of 5600 Hz. This frequency was altered over short times to obtain one pulse of light per photographic image. The flow was photographed with a Nikon FE2 35-mm camera and a Nikkor 2.8 55-mm lens attached to an MD-12 motor drive. Phase-locked photographs were obtained using a custom electronic circuit to link the laser pulse, speaker, and camera timing.

Single-pulse photographs of particle-laden flow were printed on 8 × 10-in. sheets of paper and scanned into a Macintosh II computer. Software transformed the resulting image into a full bit-map representation. All contiguous objects in the bit-map file were identified and classified according to the pixel area and moment of inertia. These parameters were used to differentiate between particles, fiducial marks, and stray objects. For a single particle, the pixel area could vary from 1 to over 50, depending on the particle position within the cross section of the laser sheet. The image moment of inertia was employed to differentiate round objects from elongated ones and in particular to help identify overlapping particles. Hence number density in areas of high particle concentration would not be underestimated.

Files of particle positions were converted into maps of number density based on a rectangular grid of points spaced at 2-mm intervals. The number densities at the four grid points surrounding each particle were incremented according to the exact particle position. For example, if a particle were equidistant from the four nearest grid points, the number density associated with each point would be incremented by one-fourth. Each map was normalized by the total number of particles counted. Photographs covered the range

Fig. 2 Unforced particle-laden flow, $Re_D = 1.9 \times 10^4$.

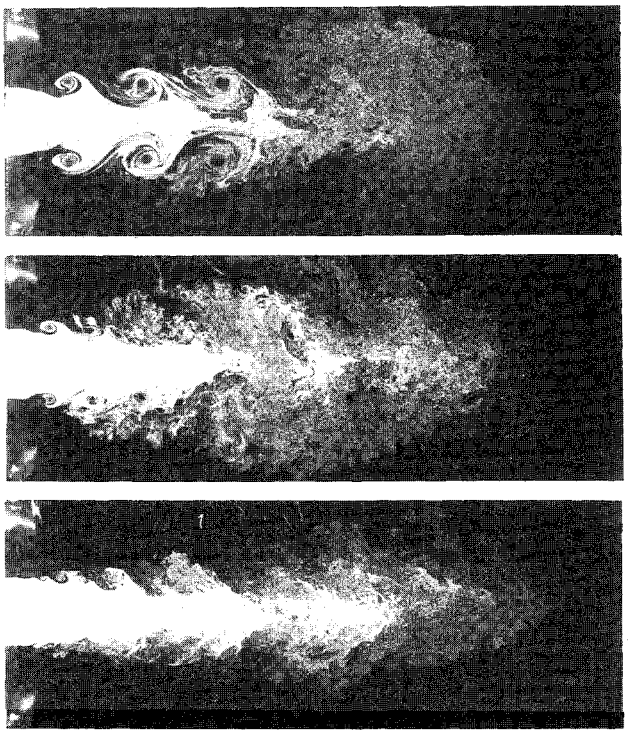

Fig. 3 Single-phase flow: St_D = 0.5 (top), St_D = 0.9 (middle), and unforced (bottom).

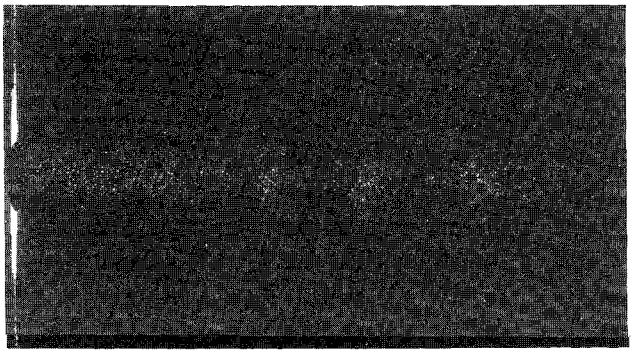

Fig. 4 Particle-laden flow, St_D = 0.5.

$x/D < 8$ and $r/D < 3.0$ and typically contained about 1700 particles. Results from 25 photographs were summed and normalized for each case of flow studied.

Particle velocities were measured with a TSI single-component laser Doppler anemometer set up in back scatter. The optics could be aligned to measure either axial or radial particle velocities. The measuring volume had a length and a diameter of 0.38 and 0.053 mm, respectively. For the radial velocity measurements, one beam was Bragg shifted to eliminate directional ambiguity.

Time-averaged velocity measurements were computed by acquiring sets of 2000 samples from a counter processor at a sampling rate of 20 Hz. Data rates near the jet centerline were in the range 400–1200 counts per second but decreased sharply with increasing radius. Radial traverses moving away from the jet axis were cut off when the data rate dropped below 20 counts per second. Near the jet centerline, where data rates were high, it is expected that velocities of particles were sampled at random times compared with the passage of vortex ring structures. Where data rates were low, however, velocities of particles from areas of high concentration were sampled preferentially since the processor was updated only when a new particle traversed the measuring volume. Thus, if many more particles were present in vortex braid regions than in vortex cores, and the data rate was on the same order as the sampling rate, almost no particles from the core regions were sampled. Maximum values of statistical uncertainties in time-averaged mean velocity measurements were 0.6% for axial particle velocities and 0.05 m/s for radial particle velocities. The uncertainty in the variance was 6% for both axial and radial velocities. The total uncertainty in mean time-averaged velocity measurements, dominated by the uncertainty due to flow unsteadiness, was estimated as 4%.

Results

The jet was qualified in single-phase flow with a single hot wire. The mean velocity profile exiting the nozzle had a top-hat shape, and the level of fluctuations in the jet core was less than 1%. The momentum thickness of the shear layer at this axial position was computed as $\Theta_m = 0.16$ mm, yielding a preferred roll-up frequency for the jet of 1500 Hz.[20]

Figure 2 shows smoke-marked, particle-laden flow in the unforced jet. Axisymmetric structures are present near the nozzle exit. These structures typically grow and pair into larger structures as they progress downstream. By x/D of 3, the structures appear more helical. Over the range shown ($x/D < 6$), the axial length scale of the structures increases by more than an order of magnitude. Hence a substantial variation in structure size normally exists over this range.

Upon exiting the nozzle, most of the particles are concentrated near the center of the jet core. This is a result of particles attaining inward radial velocities through the first half of the contraction and

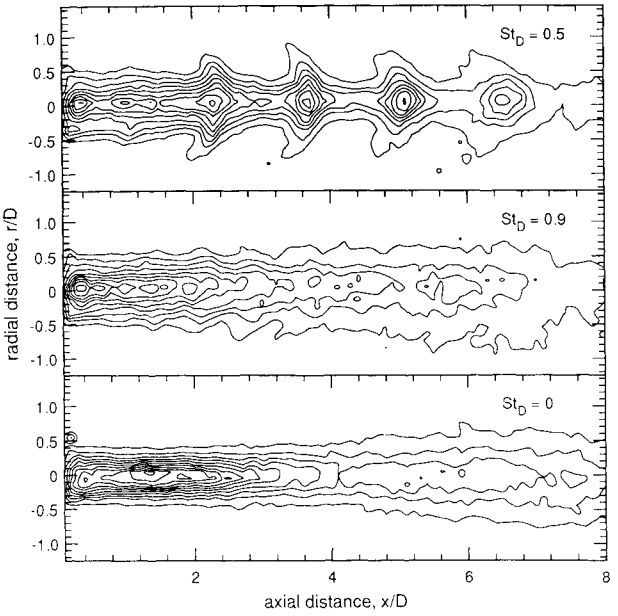

Fig. 5 Particle number density maps: St_D = 0.5, 0.9, and unforced flow. Lowest contour level is 0.0002. Succeeding levels are incremented by 0.0004.

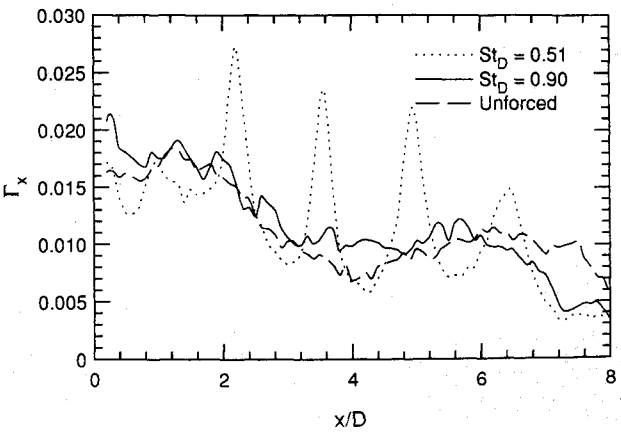

Fig. 6 Γ_x vs x/D: St_D = 0.5, 0.9, and unforced flow.

continuing to move inward through the second half. Initially, then, most particles do not interact with the vortices rolling up in the shear layer. As the vortices grow, however, they begin to entrain some particles. Starting at $x/D = 2$, particles are convected outward on the downstream side of a vortex core. At this location, the Stokes number is about 10. Further downstream, where St is 5 or less, the structures are capable of deflecting the entire particle stream. Also, some particles are ejected outward beyond the limits of the smoke. Analysis of numerous photographs reveals that these particles often continue to move outward from the jet axis. In an earlier paper, we concluded that this is the dominant mechanism for particle dispersion in a natural jet.

Single-Frequency Forcing

The first means of control applied to modify particle dispersion in the jet was single-frequency forcing. The forcing frequency was varied over a range of Strouhal numbers ($St_D = fD/U_0$) from 0.3 to 1.1. Forcing amplitudes at lower frequencies were larger as these

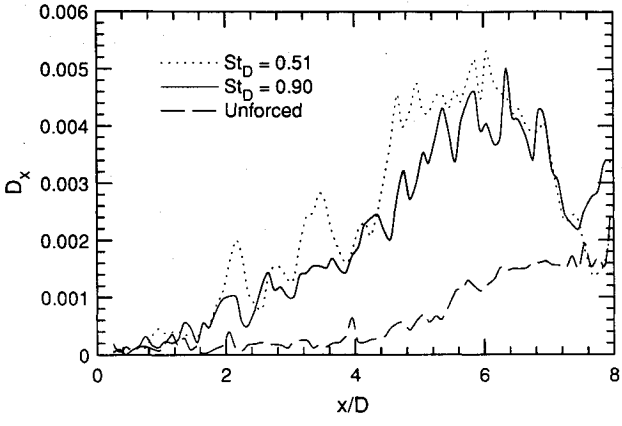

Fig. 7 D_x vs x/D: $St_D = 0.5$, 0.9, and unforced flow.

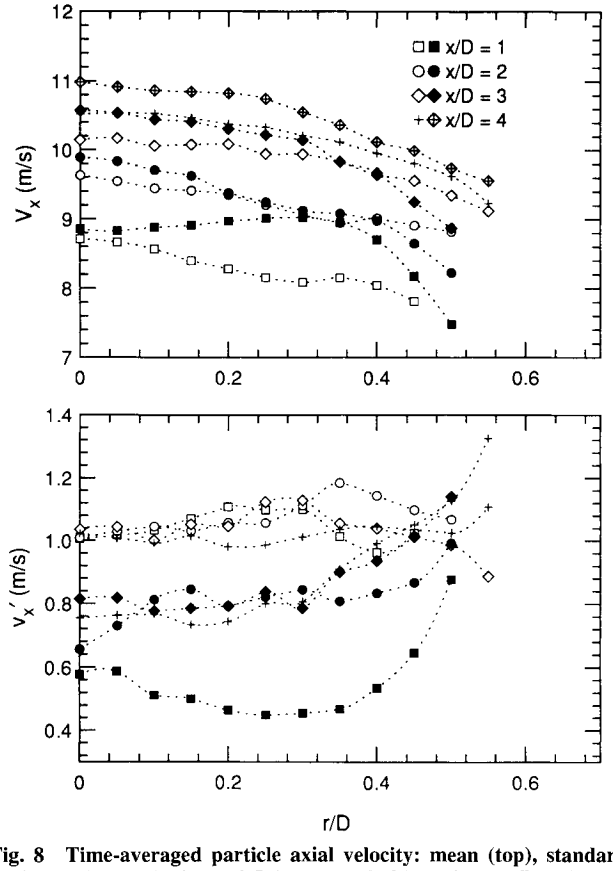

Fig. 8 Time-averaged particle axial velocity: mean (top), standard deviation (bottom); $St_D = 0.5$ (open symbols), unforced flow (closed symbols).

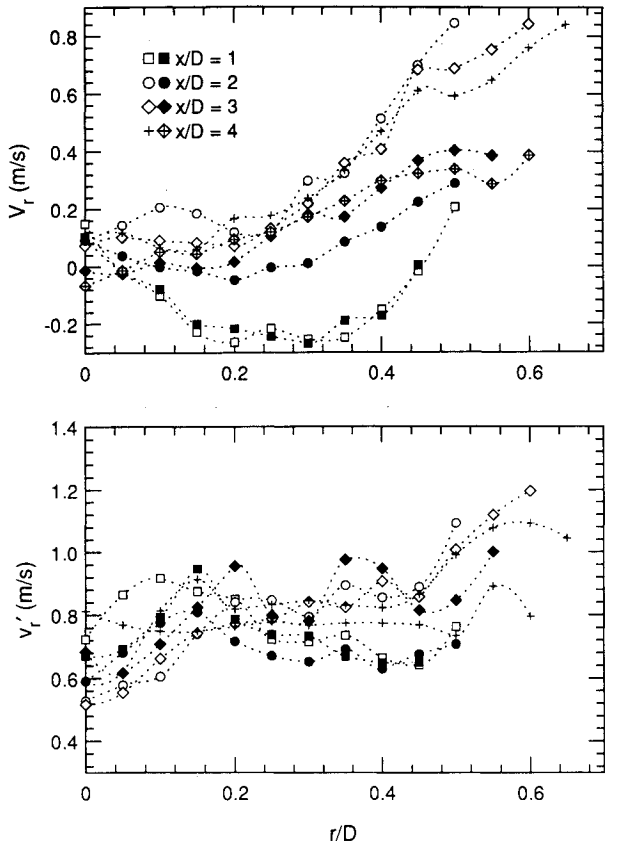

Fig. 9 Time-averaged particle radial velocity: mean (top), standard deviation (bottom); $St_D = 0.5$ (open symbols), unforced flow (closed symbols).

frequencies lay further from the most amplified frequency as determined by linear stability analysis. For $St_D = 0.5$ and 0.9, the forcing yielded nozzle exit velocity fluctuations of $u'/U_0 = 0.11$ and 0.045, respectively. Single-phase flow forced at these frequencies is shown in Fig. 3 next to a photograph of unforced flow. When $St_D = 0.5$, large vortex rings form and propagate downstream so that a constant spacing between neighboring cores is maintained. As the forcing frequency increases, the size of the vortex rings and the spacing between them decrease. Note that the larger rings in the $St_D = 0.5$ case disturb a much larger portion of the jet's potential core than the smaller rings in the $St_D = 0.9$ case. Also, the smaller rings in the high-frequency case either pair or appear to lose their coherence sooner than those in the low-frequency case. Videotape superposition of numerous images of the same phase of flow shows that strong coherence from the smaller rings generally does persist downstream to the limit of the laser sheet. Note also that the rings in the $St_D = 0.9$ case are larger than those initially forming in unforced flow.

Photographs of the identical phase of particle-laden flow were taken of each case. Figure 4 depicts an example for $St_D = 0.5$. Along the jet axis, areas of relatively high particle concentration are interspersed with areas of lower concentration. Videotapes of this and similar cases indicate that particles are dispersed outward from the jet axis near the areas of high concentration. Also, the areas of high concentration correspond to the regions of high strain downstream of vortex cores. Photographs of unforced flow show very few particles that have dispersed far from the jet axis.

Contour maps of normalized particle number density for $St_D = 0.5$ and 0.9 and unforced flow are plotted in Fig. 5. Maps of forced flow, computed for a specific phase of forcing, show the effects of structure on instantaneous particle distribution, but in the unforced case, the effects of structure are averaged out. When the forced and unforced cases are compared, it is clear that axial forcing alters the initial distribution of particles exiting the nozzle. In both cases shown, forcing increases the radial spread of particles at the nozzle exit. Although variations are smeared out, particles in the unforced

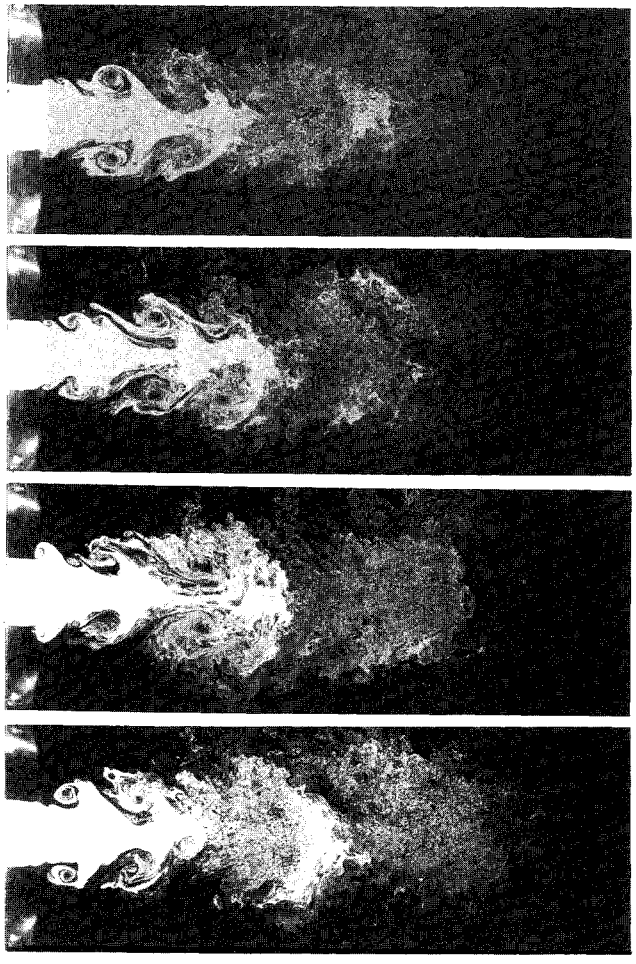

Fig. 10 Single-phase flow, $St_D = 0.5 + 0.25$, $\Theta = 30$ deg (case L): phase I (top) to phase IV (bottom).

jet appear to remain tightly collimated. The local number density decreases monotonically with increasing x and r. Also, low-level contours extend further downstream than in forced flow, indicating that relatively fewer particles have dispersed before $x/D = 8$.

The $St_D = 0.9$ case is similar to unforced flow in that, near the jet axis, number density decreases monotonically with increasing axial distance and the contours follow relatively straight paths. The outer contours are wavy, however, due to the presence of phase-locked vortex rings. The wavelength of these contours matches the vortex ring spacing, and the locations where the contours bend inward correspond to the ring core positions. Also, the contours are spread across a greater diameter than in the unforced case. The $St_D = 0.5$ case differs radically from the unforced case. Here, the larger vortex rings cause the particles to form clusters of high number density. Between the clusters are areas of relatively low number density, and the contours are pinched in compared with the other cases. The structures are strong enough that particles move in the axial direction out of streaming regions inside of each vortex ring and into the straining regions between the rings. In the cluster centers, the local number density is sometimes larger than at the jet exit. Note also that the clusters have tails where particles have been displaced outwards by outwardly moving fluid downstream of the vortex rings. The clusters move downstream at the vortex propagation velocity of $0.7U_0$ so that a constant spacing is maintained.

The statistic Γ_x was defined as the sum of the number density values at a given axial position. This statistic weights the inner portions of the jet because the total azimuthal angle intercepted by the laser sheet decreases with increasing radius. Thus, Γ_x tends to decrease with increasing x as particles move away from the jet axis. Nevertheless, Γ_x provides a good quantitative measure of the axial clustering observed in the number density maps. Figure 6 shows Γ_x for the three cases described earlier. This plot shows definitively for $St_D = 0.5$ that the generation of large structures causes strong axial displacement of particles into regions of high particle density. The peak levels for this case are much higher than Γ_x near the nozzle exit. Also, the local minima drop below the corresponding levels in the unforced case. Hence, this means of control yields areas of both high and low particle number density. The value of Γ_x drops off beyond a peak at $x/D = 6$. From photos of this case and another taken 180 deg out of phase, it appears that a large percentage of all particles has dispersed or moved away from the jet axis by this axial location. Also, for this case, particles attain sufficient radial velocities to escape the camera field of view by $x/D = 5$.

The $St_D = 0.9$ case, which contains more frequent vortices with smaller cores, also shows variations in Γ_x corresponding to the distance between successive flow structures. This plot lies closer to Γ_x for unforced flow. Like the $St_D = 0.5$ case though, Γ_x drops off sharply beyond x/D of 7 compared with unforced flow. Again this indicates that particles have dispersed faster in forced than in unforced flow.

A particle moment function D_x was computed to quantify radial dispersion:

$$D_x = \int_{0.5}^{3} cr \, dr$$

In this definition, c is the local number density, and r is the radius. The lower limit is set at 0.5 rather than 0 in an attempt to distinguish dispersion effects from clustering near the jet axis. Even though this statistic (plotted in Fig. 7) ignores particles near the jet axis, some effect of clustering at the vortex ring spacing is still apparent for both $St_D = 0.5$ and 0.9. For $St_D = 0.9$, peaks occurring at the vortex ring spacing are aligned approximately with the local maxima in Γ_x. For $St_D = 0.5$, however, the peaks downstream of $x/D = 3$ are located slightly upstream of peaks in Γ_x, suggesting

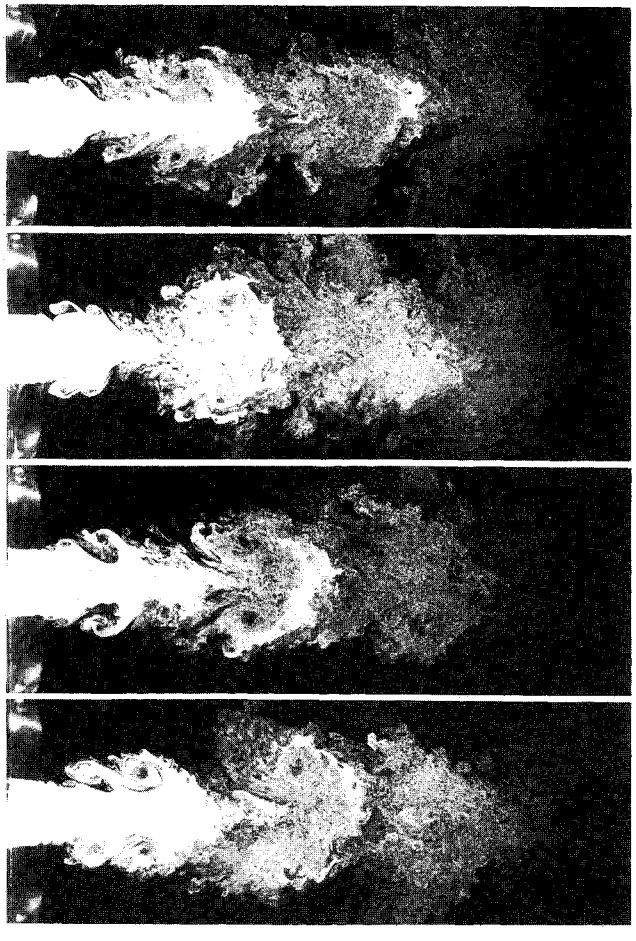

Fig. 11 Single-phase flow, $St_D = 0.5 + 0.25$, $\Theta = 120$ deg (case E): phase I (top) to phase IV (bottom).

that in an instantaneous view the ejected particles lag the areas of high particle concentration near the jet axis. Since axial velocities of ejected particles will decrease in areas of low fluid velocity, this is not surprising.

For $x/D < 6$, the dispersion for both forced cases greatly exceeds the unforced case. The plots of D_x for forced flow actually drop off after x/D of 6 because some particles have passed out of the camera field of view. In contrast, almost all particles in the natural jet remain within $r/D < 1.5$. When D_x is integrated over x for $x/D < 8$, the dispersion for the case with larger vortices exceeds the higher frequency case by 19%. Over this range, the integrated values of D_x are 0.19, 0.16, and 0.05 for $St_D = 0.5$ (average of two phases), 0.9, and unforced flow. For $0 < x/D < 6$, the integrated values for D_x are 0.13, 0.10, and 0.022, respectively, representing even larger differences between the cases. It appears, then, that early generation of vortices larger than those occurring in a natural jet increases particle dispersion, with particles dispersing faster when vortices are larger. This conclusion cannot be generalized to larger or smaller particles, and so it must be restricted for now to the range $6 < St < 20$.

Time-averaged statistics were computed from LDA measurements to compare particle velocities in the $St_D = 0.5$ and natural cases. Axial and radial particle velocity profiles are plotted in Figs. 8 and 9. The forcing causes slight decreases in the axial particle velocity for $x/D < 4$. Over this range, particles in the jet core are accelerating after exiting the jet nozzle. Hence, forcing decreases particle accelerations downstream of the jet nozzle on average. Otherwise, the mean axial velocity profiles in both cases have similar shapes. The standard deviation in axial particle velocity is increased by the forcing, which is expected since the rms fluid velocity is significantly larger for forced flow. The most obvious differences between the two cases occur in the mean radial velocities. At $x/D = 1$, negative radial velocities are present as the particles continue to move inward after exiting the contraction. Further downstream, however, forcing causes significantly increased positive radial velocities as we move away from the jet axis. Radial velocities for $r/D < 0.2$ are comparable for the two cases. The plots of the standard deviation in radial particle velocity show no meaningful differences between forced and unforced flow.

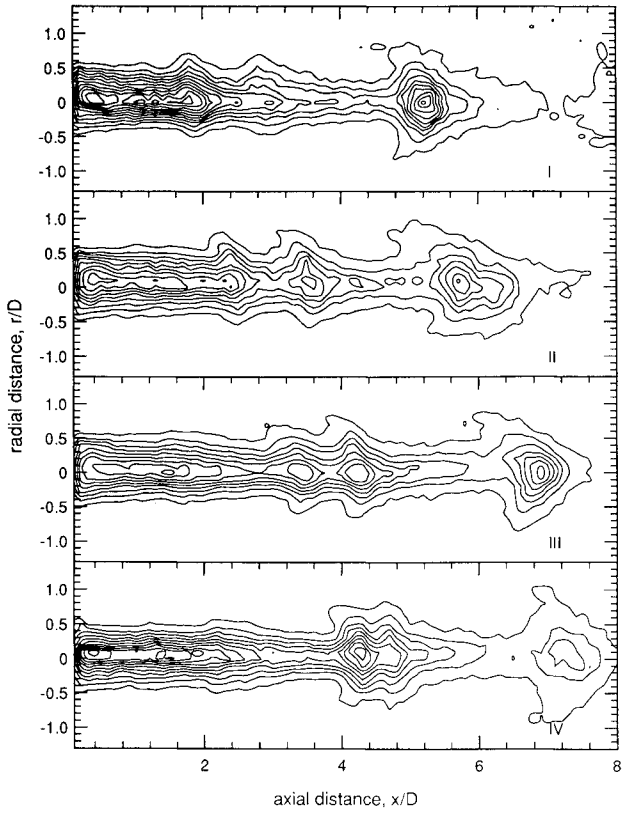

Fig. 12 Particle number density maps: $St_D = 0.5 + 0.25$, $\Theta = 30$ deg (case L).

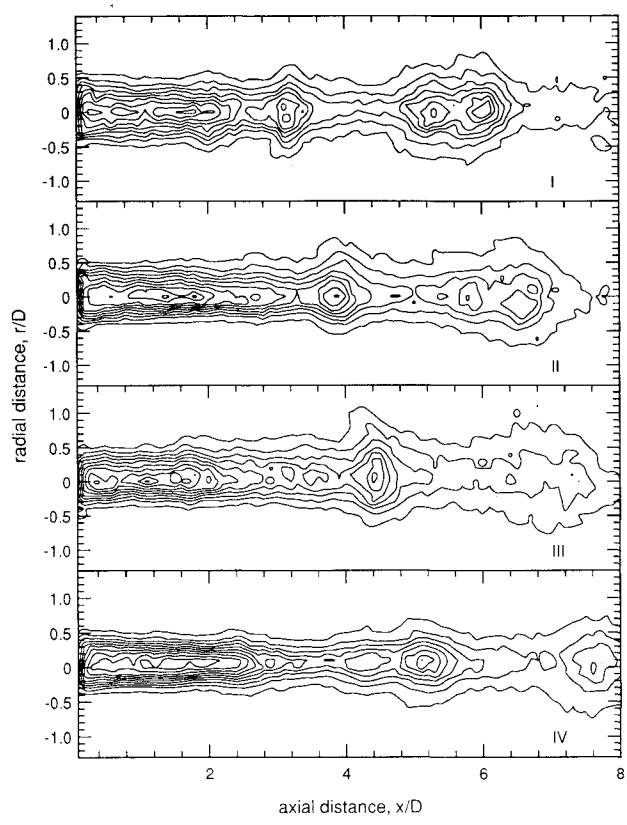

Fig. 13 Particle number density maps: $St_D = 0.5 + 0.25$, $\Theta = 120$ deg (case E).

Double-Frequency Forcing

A second means of dispersion control was examined whereby the jet was forced simultaneously at two frequencies, a fundamental and its first subharmonic. Here, the relative phase between the two frequencies becomes important. The double-frequency forcing generally causes a pairing between two vortices that form at the fundamental frequency. The relative phase between the two forcing signals plays a significant role in determining the location and nature of this pairing. If vortex pairing affects local particle motion, then the phase variation can be used to exert control over the axial locations of dispersion.

The effects of relative and overall forcing amplitude on particle-laden flow are not addressed in the present work. In single-phase flow, however, we find that as overall forcing amplitude and hence periodic velocity fluctuation levels are increased, the range of possible pairing locations also increases. At one extreme, the upstream vortex of a given pair fails to catch its downstream counterpart before the rings lose coherence. At the other extreme (at high forcing levels), the two rings pair almost immediately after they form.

The current discussion focuses on cases forced at $St_D = 0.5$ and 0.25, where the composite signal entering the speaker can be represented by

$$A = \sin(2\pi ft) + \sin(\pi ft + \Theta) \tag{1}$$

Two cases that approach the pairing extrema for a moderate forcing level are examined: $\Theta = 120$ deg, which yields an early pairing (case E), and $\Theta = 30$ deg, which yields a late pairing (case L). The forcing amplitudes yielded u'/U_0 of 0.11 and 0.09 for cases E and L, respectively. The 90-deg phase shift in Θ yields waveforms that are mirror images about the amplitude axis. (The composite waveforms are also displaced by 180 deg in time, which is considered irrelevant to our results.) These waveforms differ from those originally generated in the computer due to phase shifts occurring in both the amplifier and filter. Smoke-marked flow for both cases is depicted in Figs. 10 and 11. (In these and subsequent figures, four

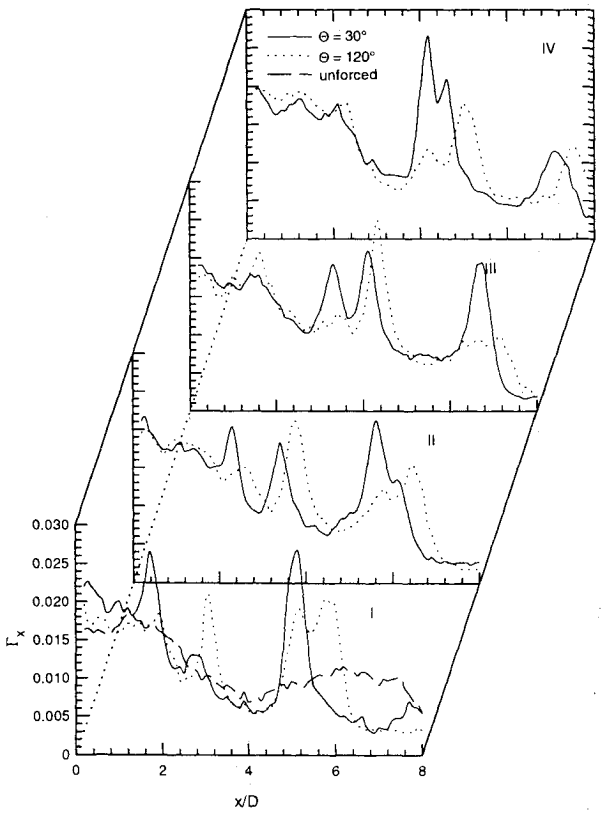

Fig. 14 Γ_x vs x/D: $St_D = 0.5 + 0.25$.

equally spaced phases of the forcing cycle are shown). These photographs, as well as videotapes of strobed flow, show pairs of vortices forming at the fundamental frequency. Initially, the vortices in each pair appear similar in size. When $\Theta = 30$ deg, however, the upstream member of each pair is relatively weaker (contains less circulation). Hence, it propagates more slowly and takes longer to catch the downstream ring. Once the upstream vortex moves inside the core of its counterpart, it appears to break down. In contrast, when $\Theta = 120$ deg, the upstream ring of each pair is relatively stronger. It catches its downstream counterpart more quickly and persists, leapfrogging through the other ring's center. Vortex pairing occurs at $x/D = 3.3$ for case E and 3.7 for case L.

Contour plots from the corresponding particle-laden flow cases are shown in Figs. 12 and 13. In Fig. 12, a pair of clusters at x/D of 1.8 and 2.9 is present in plot I. The clusters propagate downstream, pairing into a very dense cluster at x/D of 5.2. Although the initial particle clusters appear weaker than in the single frequency $St_D = 0.5$ case, the paired cluster is larger with a greater number density at its center. Compared with the cluster at $x/D = 5$ in the $St_D = 0.5$ case, the maximum number density in the merged cluster is greater by 27%. This dense cluster retains its shape as it moves downstream to the limit of the illuminated range. Cusps on the upstream edges of the cluster indicate the location of substantial and steadily ongoing particle dispersion.

Case E in Fig. 13 was found to produce sets of two vortices that leapfrogged at x/D of 3.3. In the uppermost contour plot, two weak particle clusters are apparent at $x/D = 2$ and 3.2. However, as we progress forward in time, only one distinct cluster can be seen. This strong cluster is located at $x/D = 4.5$ in plot III, which is slightly downstream of the approximate vortex pairing position. At this point, the radial spread of the number density contours is maximized. Then the cluster elongates as it continues downstream. By $x/D = 5.6$, the distribution of particle number density within the cluster is clearly bimodal. This distribution probably occurs due to the leapfrogging vortex rings. Just as two clusters merge into one as the vortex rings merge, the single cluster is redistributed into two (or a single bimodal cluster) as the rings separate.

The contours in Fig. 13 indicate that the bimodal cluster is longer, rounder, and less concentrated than the paired cluster in Fig. 12. Unlike in case L, no cusps are present on the bimodal cluster as it propagates downstream. Although the number density within the cluster decreases steadily from x/D of 5 to 8, the mechanism for particle dispersion is unknown. Perhaps particles are propelled away from the jet at more than one axial location relative to the cluster. Then the number of particles ejected at a single location may be insufficient to appear on the plots.

Figure 14 shows Γ_x plotted for both subharmonic forcing cases. For case L, sets of two peaks corresponding to two initial particle clusters are visible. The peaks eventually merge into one large, relatively sharp peak near $x/D = 5$ (plot I), which persists as the corresponding cluster continues downstream. Case E shows some clear differences. In plot I, two peaks are present at x/D of 1.8 and 3 where the downstream peak is stronger, suggesting that the downstream cluster contains more particles than its counterpart. In plot III, the downstream peak completely dominates, reaching a maximum for all of the phases examined. This maximum is significantly lower than that occurring for case L. This is the location where, in Fig. 13, a single cluster exists downstream of the vortex pairing location. Further downstream, the bimodal cluster maps into a bimodal peak in Γ_x, which is much broader than the corresponding peak for case L.

Figure 15 displays plots of radial dispersion D_x for both cases. Note that these plots are relatively noisy because particles farther from the jet axis make larger contributions to D_x. Since relatively few particles were counted far from the jet axis, statistical variations are larger. For case L, broad peaks are centered slightly upstream of peaks seen in Γ_x, most likely the result of particle ejections from clusters. For case E, the peaks are smaller and narrower, indicating that earlier pairing of rings is less effective at dispersing particles than later pairing. In both cases, the radial dispersion integrated over x for $x/D < 8$ sums to values (averaged over four phases) lying between those for unforced and single-frequency forced flow. The values are 0.12 for case L and 0.07 for case E. For $0 < x/D < 6$, the integrated values are 0.07 and 0.04 for cases L and E. Although we have examined only a limited number of cases, these results may imply that close to the jet exit, fewer particles are ejected from the jet inner region in flow forced with subharmonics than in flow forced with a single frequency. By encour-

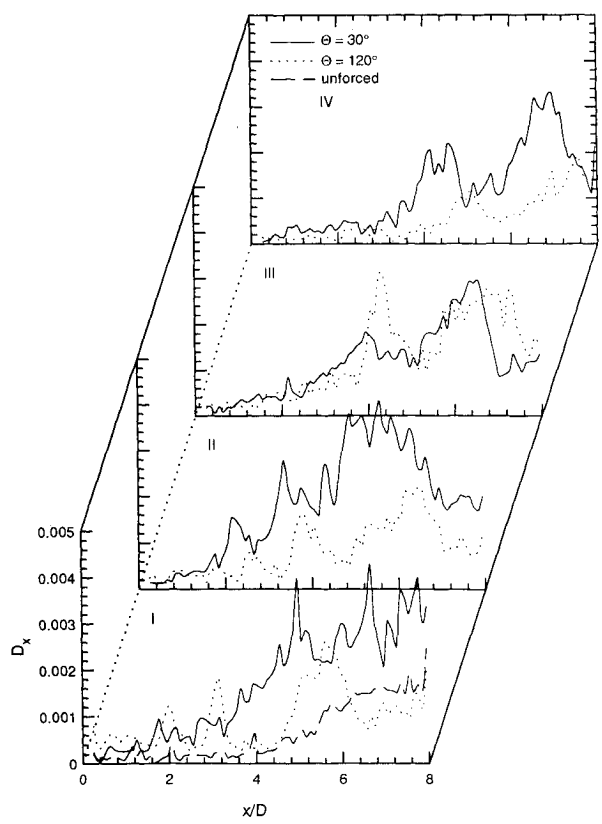

Fig. 15 D_x vs x/D: $St_D = 0.5 + 0.25$.

aging an earlier pairing of ring vortices (case E), dispersion is further reduced compared with case L with a later pairing.

Discussion

Other than forcing frequency, factors that affect dispersion that were not addressed systematically in this study are forcing amplitude, initial particle distribution and velocity, and particle-particle interactions. In the present research, forcing amplitudes chosen represented the minimum levels needed to produce the appropriate collective interactions. If those amplitudes were increased, thus increasing the amplitudes of periodic velocity fluctuations, we suspect that particle dispersion would be altered. Specifically, the velocities of particles ejected from the jet should change in magnitude and direction. Also, increased amplitudes applied to multiple frequency forced cases should yield greater possible variations in pairing locations and processes as differences in the strength of vortices originally forming at the fundamental frequency increase.

In terms of initial conditions, the results described here stem from flow exiting a contraction. Although air exiting the contraction is aligned with the jet axis, particles have significant negative radial velocities. Also, particles exiting the contraction lag the fluid so that initial particle Reynolds numbers are significant ($Re_p \sim 3$). Since many particles have negative radial velocities at the jet exit and others are already located near the jet axis, we expect dispersion to be delayed compared with an idealized case of zero radial velocity and uniform distribution. On the other hand, the fact that particles initially lag the fluid may enhance dispersion. For a particle to disperse, it must be accelerated radially by outwardly moving fluid. Also, the particle must attain a radial velocity large enough to escape the vortex core region and avoid becoming re-entrained in the jet.

Consider a particle moving near the jet axis that encounters a ring vortex (Fig. 16). The vortex propagates at about $0.7U_0$, and we examine a reference frame moving with the vortex. To escape the jet, a particle with relative axial velocity v_x must be accelerated outward in the region of length $L/2$ downstream of the vortex core where u_r is positive. The radial particle acceleration is

$$\frac{dv_r}{dt} = \frac{f}{\tau_p}(u_r - v_r) \tag{2}$$

where the only force on the particle is assumed to be a modified Stokes drag with $f = 1 + 0.15\mathrm{Re}_p^{.2/3}$ In the simplest analysis, we can assume that u_r, v_x, and f are constant over this range, and that v_r is initially zero. Then, Eq. (2) integrates to

$$v_r = u_r\left[1 - \exp\left(\frac{-ft}{\tau_p}\right)\right] = u_r\left[1 - \exp\left(\frac{-fx}{\tau_p v_x}\right)\right] \tag{3}$$

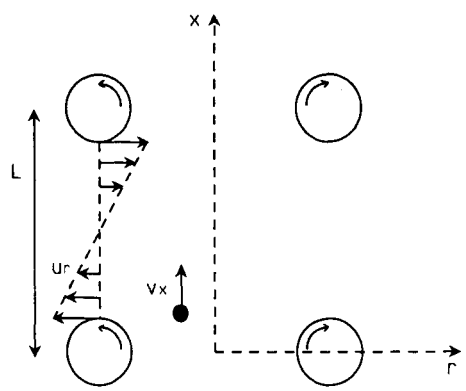

Fig. 16 Particle passing between ring vortices. Circles represent cross sections of vortex cores; U_r is fluid velocity and V_x is particle velocity; and both are relative to the core center.

where $x = v_x t$. This result illustrates two key points. First, smaller values of v_x (with respect to the vortex) will yield larger values of v_r. Second, larger values of L, corresponding to increased vortex spacing, will allow a radial acceleration to be applied over a longer time. If particles near the jet centerline initially matched the jet exit velocity in the current experiments, v_x would be larger than 5 m/s, meaning that particles near the jet axis would fly by vortices without being diverted significantly. The actual conditions, however, yield $v_x \sim 1$ m/s or less. Particles move at axial velocities very close to the vortex propagation velocity and can accumulate in the straining regions downstream of vortices. Eventually, they are pulled outward. These conditions allow acceleration over a significant time (> 10 ms) and most likely increase particle ejections in the jet near field.

Although these experiments were performed at relatively low volumetric loadings, it appears that particle-particle interactions could become significant in particle clusters under moderate loadings. When particles located very close to one another are subject to variations in fluid velocity, drag characteristics may differ from those assumed for isolated spheres. Furthermore, in reacting flows, particle-particle interactions would affect evaporation and reaction rates (see Bellan and Harstad,[21] for example). Thus, control of particle motion in reacting flows may be as concerned with controlling areas of particle concentration as with controlling overall dispersion rates. Where rapid dispersion of particles may be desired in a lean burning combustor, early concentration of particles may be desired in a two-stage, rich-then-lean combustor.

Summary

The results show clearly that, for particles with appropriate inertial time constants, control of the scale and nature of ring vortices in the flow can be used to modify particle dispersion. Single-frequency forcing over a range of Strouhal numbers can be used to control the extent to which particles form clusters as well as to increase particle dispersion in the jet near field. The forcing also regulates the rate and nature of particle dispersion by specifying the frequency of locations at which significant dispersion occurs and to some extent the velocity at which particles are ejected. Hence, the radial extent of dispersion is somewhat controllable. Forcing with two frequencies—a fundamental and a subharmonic—allows control of vortex pairing. This type of forcing allows the formation of even denser particle clusters if desired. Also, locations of strong dispersion can be delayed compared with the single frequency cases. Furthermore, variation of the phase between the two forcing waves allows some control of the vortex pairing location as well as the nature of cluster merging and subsequent dispersion.

Acknowledgments

This work was funded by the Electric Power Research Institute under Contract RP 8005-2 monitored by George Offen. The first author was supported by fellowships from the Link Foundation and the American Association of University Women.

References

[1]Crow, S. C., and Champagne, F. H., "Orderly Structure in Jet Turbulence," *Journal of Fluid Mechanics*, Vol. 48, 1971, pp. 547–591.

[2]Yule, A. J., "Large-scale Structure in the Mixing Layer of a Round Jet," *Journal of Fluid Mechanics*, Vol. 89, Pt. 3, 1978, pp. 413–432.

[3]Petersen, R. A., and Samet, M. M., "On the Preferred Mode of Jet Instability," *Journal of Fluid Mechanics*, Vol. 194, 1988, pp. 153–173.

[4]Mungal, M. G., and Hollingsworth, D. K., "Organized Motion in a Very High Reynolds Number Jet," *Physics of Fluids A*, Vol. 1, No. 10, 1989, pp. 1615–1623.

[5]Yule, A. J., Chigier, N. A., Ralph, S., Boulderstone, R., and Ventura, J., "Combustion-Transition Interaction in a Jet Flame," *AIAA Journal*, Vol. 19, No. 6, 1981, pp. 752–760.

[6]Koch, C. R., Powell, J. D., and Reynolds, W. C., "Closed Loop Control of a Round Jet/Diffuser in Transitory Stall," Ph.D. Dissertation, Dept. of Mechanical Engineering, Stanford Univ., Stanford, CA, 1990.

[7]Ho, C. M., and Gutmark, E., "Vortex Induction and Mass Entrainment in a Small-Aspect-Ratio Elliptic Jet," *Journal of Fluid Mechanics*, Vol.

179, 1987, pp. 383–405.

[8]Wlezien, R. W., and Kibens, V., "Passive Control of Jets with Indeterminate Origins," *AIAA Journal*, Vol. 24, No. 8, 1986, pp. 1263–1270.

[9]Hussain, A. K. M. F., and Zaman, K. B. M. Q., "The 'Preferred Mode' of the Axisymmetric Jet," *Journal of Fluid Mechanics*, Vol. 110, 1981, pp. 39–71.

[10]Reynolds, W. C., and Bouchard, E. E., "The Effect of Forcing on the Mixing Layer Region of a Circular Jet," *Unsteady Turbulent Shear Flows*, Springer, New York, 1981, pp. 401–411.

[11]Lee, M., and Reynolds, W. C., "Bifurcating and Blooming Jets," Thermosciences Division, Dept. of Mechanical Engineering, Stanford Univ., Rept. TF-22, Stanford, CA, Aug. 1985.

[12]Ho, C. M., and Huang, L.-S., "Subharmonics and Vortex Merging in Mixing Layers," *Journal of Fluid Mechanics*, Vol. 119, 1982, pp. 443–473.

[13]Arbey, H., and Ffowcs Williams, J. E., "Active Cancellation of Pure Tones in an Excited Jet," *Journal of Fluid Mechanics*, Vol. 149, 1984, pp. 445–454.

[14]Mankbadi, R. R., "The Effect of Phase-Difference on the Spreading Rate of a Jet," *AIAA Journal*, Vol. 24, No. 12, 1986, pp. 1941–1949.

[15]Husain, H. S., Bridges, J. E., and Hussain, A .K .M. F., "Turbulence Management in Free Shear Flows by Control of Coherent Structures," *Transport Phenomena in Turbulent Flows*, edited by Hirata and Kasagi, Hemisphere, New York, 1988, pp. 111–130.

[16]Lazaro, B. J., and Lasheras, J. C., "Particle Dispersion in a Turbulent, Plane Shear Layer," *Physics of Fluids A*, Vol. 1, No. 6, 1989, pp. 1035–1044.

[17]Kamalu, N., Wen, F., Troutt, T. R., Crowe, C. T., and Chung, J. N., "Particle Dispersion by Ordered Motion in Turbulent Mixing Layers," *ASME Forum on Cavitation and Multiphase Flow*, 1988, pp. 150–154.

[18]Longmire, E. K., and Eaton, J. K., "Structure of a Particle-Laden Round Jet," *Journal of Fluid Mechanics*, Vol. 236, 1992, pp. 217–257.

[19]Longmire, E. K., and Eaton, J. K., "Structure and Control of a Particle-Laden Jet," Thermosciences Division, Dept. of Mechanical Engineering, Stanford Univ., Rept. MD-58, Stanford, CA, Sept. 1990.

[20]Michalke, A., "On Spatially Growing Disturbances in an Inviscid Shear Layer," *Journal of Fluid Mechanics*, Vol. 23, 1965, pp. 521–544.

[21]Bellan, J., and Harstad, K., "Burning of Dense Clusters of Fuel Drops," Jet Propulsion Lab., New Technology Rept. NPO-17987/7487, Pasadena, CA, 1992.